Progress In Electromagnetics Research B, Vol. 76, 111–123, 2017

Fast Design of Asymmetrical Permanent Magnet Synchronous Machines that Minimize Pulsating Torque

Alejandro J. Piña Ortega*

Abstract—Torque pulsations in Permanent Magnet Synchronous Machines are mainly created by interaction between the permanent magnets and stator teeth, harmonics in the stator current, steel saturation and partial magnet demagnetization. As a consequence of torque ripple, there are increased noise and vibrations. To overcome them, some methods for reducing pulsating torque include controlled-asymmetry. The strategy seeks for compensate or cancel out spatial harmonics of flux density in the air gap. This work proposes an analytical method based upon sub-domain model that allows techniques such as stator teeth pairing, slot opening shift, nonuniform teeth, tangential shift of magnets, different magnet widths, among others, to be utilized and motor performance quickly analyzed. Since asymmetries introduce several degrees of freedom, the design of Permanent Magnet Synchronous Machines can be accelerated by means of analytical-based tools. The proposed model is validated with Finite Element method.

1. INTRODUCTION

Nowadays, the pursuit of a greener lifestyle accompanied by the increase of population growth worldwide has set new challenges in the demand for low-carbon electricity. The conventional modes of generation and consumption of electrical energy have been experiencing changes in the last decade due to advances in power electronics, and nevertheless, there still exist radical approaches yet to be evaluated or implemented before being able to supply the future need for clean energy.

Electric machines (e-machines) are one of the key enabling technologies that can determine success or failure on supplying the future demand. Hence, the design, analysis, control and diagnosis of e-machines are deemed as a reemerging research field. The prevailing power density (kW/kg) and efficiency of e-machines are among the constraints that need to be overcome and have been the center of attention for researchers worldwide.

Permanent Magnet Synchronous Machines (PMSMs) merge the aforementioned topics by allowing researchers and designers to employ materials with high self-contained energy-product (rare-earth magnets) and steel alloys, into creative geometries that require the machines to be carefully operated in order to avoid permanent demagnetization.

In PMSM, torque pulsations are mainly created by interaction between the permanent magnets (PMs) and stator teeth, harmonics in the stator current, steel saturation and partial magnet demagnetization. Noise, vibration and losses are usually byproducts of high pulsating torque. Methods for reducing torque pulsations have been extensively studied, in which emphasis has been put on compensating or canceling out spatial harmonics of flux density in the air gap so that smoother torque is achieved. In the last decade, several studies have been presented where researchers introduced controlled-asymmetry with the aim of reducing pulsating torque, particularly, cogging torque has been mainly analyzed since it is a measure of undesired pulsations that also adds up to the overall torque production.

Received 19 March 2017, Accepted 8 June 2017, Scheduled 23 June 2017
* Corresponding author: Alejandro J. Pina Ortega (a.pina-ortega@ieee.org).
The author is with the Research and Development at Nexteer Automotive, Saginaw, MI, USA.

With that being said, it is evident that asymmetries do not only come from manufacturing variations due to tolerances, but they can also be deliberately introduced by the designer [11]. Some examples of controlled-asymmetries are: stator teeth pairing [6], slot opening shift [8], nonuniform teeth [14], tangential shift of magnets [1, 2, 4, 15, 16], different magnet widths [13] and uneven placement of flux barriers in PM assisted synchronous reluctance motors [3].

In introducing additional degrees of freedom such as stator and rotor asymmetries, the design and analysis process become more challenging. For instance, due to the wide range of possibilities in the machine geometry, traditional models constrain the search for the optimum design to a narrower set of feasible solutions.

In order to overcome these challenges from analytic standpoint, this paper proposes an analytical model based on complete subdomain approach to account for asymmetric geometries.

The proposed method is used to compute cogging torque of several cases of study that include 27-slots/6-poles and 36-slots/6-poles PMSMs in which the aforementioned strategies were analyzed in order to show their effectiveness when minimizing pulsating torque. Additionally, the total harmonics distortion (THD) is calculated to provide a measure of back-EMF deterioration and to serve as figure of merit for comparison of studied techniques.

2. GENERAL FORMULATION FOR PMSM WITH ASYMMETRIES

The calculation of magnetic vector potential $\vec{A}$ is a boundary value problem (BVP) that is solved by dividing the machine in subdomains and applying boundary conditions (BC). The magnetic field in each subdomain is governed by the general form of diffusion equation [5, 9]

$$\nabla^2 \vec{A} + \sigma\mu\vec{v} \times \left(\vec{\nabla} \times \vec{A}\right) - \sigma\mu\frac{\partial \vec{A}}{\partial t} = -\vec{\nabla} \times \vec{B_r} + \sigma\mu\vec{\nabla}V. \tag{1}$$

It is reduced to well-known expressions as eddy currents are ignored by means of neglecting material conductivity σ. In Eq. (1), $\vec{v}$ is the relative velocity of moving conductor, μ the scalar permeability for isotropic materials, and V the electric scalar potential. For nonconductive materials, Eq. (1) yields (2)–(4)

$$\nabla^2 \vec{A}^{(G)} = \nabla^2 \vec{A}^{(SO)} = 0 \tag{2}$$

$$\nabla^2 \vec{A}^{(M)} = -\frac{\mu_0}{r}\sum_k \left[(M_{\phi c,k} - kM_{rs,k})\cos(k\phi) + (M_{\phi s,k} + kM_{rc,k})\sin(k\phi)\right] \tag{3}$$

$$\nabla^2 \vec{A}^{(S)} = -\mu\vec{J}. \tag{4}$$

The superscripts abbreviate subdomains or regions as follows: (G) is the air gap, (M) the magnet, (SO) the slot opening, and (S) the stator slot. Inside nonmagnetic regions such as air gap, slot openings and stator slots-open circuit condition, the general diffusion form is reduced to Laplace's equation, while regions enclosing magnets or excited coils are governed by Poisson's equation.

The following expression which serves as solution for the Euler's equation comes in handy to simplify the general solutions for the flux density vector that can be obtained after solving Eq. (1) by means of Variable Separation Method (VSM). In Eq. (5), $\Lambda, \lambda, \Psi, \psi, \rho$ are free parameters while r is the radius where the solution is to be calculated

$$\mathbf{\Omega_r}\left(\Lambda, \lambda, \Psi, \psi, \rho\right) = \Lambda\left(\frac{r}{\lambda}\right)^{\rho} + \Psi\left(\frac{\psi}{r}\right)^{\rho}. \tag{5}$$

2.1. Air Gap Subdomain

The general solutions of magnetic flux density vector $(\vec{B})$ are shown in Eqs. (6)–(7)

$$\vec{B}_r^{(G)} = \sum_k a_k^{(G)}\cos(k\phi) + \sum_k b_k^{(G)}\sin(k\phi) \tag{6}$$

$$\vec{B}_\phi^{(G)} = \sum_k c_k^{(G)}\cos(k\phi) + \sum_k d_k^{(G)}\sin(k\phi), \tag{7}$$

where a_k, b_k, c_k and d_k are functions that enclose the kth Fourier coefficients of the radial $\vec{B}_r^{(G)}$ and tangential $\vec{B}_\phi^{(G)}$ components of flux density in the air gap, which are functions of radius r and spatial position ϕ, as seen in Eqs. (8)–(11). R_S is the stator inner radius and R_{MO} the magnet outer radius.

$$a_k^{(G)} = \frac{k}{r} \cdot \mathbf{\Omega_r} \left(Y_k^{(G)}, R_S, Z_k^{(G)}, R_{MO}, k \right) \tag{8}$$

$$b_k^{(G)} = -\frac{k}{r} \cdot \mathbf{\Omega_r} \left(W_k^{(G)}, R_S, X_k^{(G)}, R_{MO}, k \right) \tag{9}$$

$$c_k^{(G)} = \frac{k}{r} \cdot \mathbf{\Omega_r} \left(-W_k^{(G)}, R_S, X_k^{(G)}, R_{MO}, k \right) \tag{10}$$

$$d_k^{(G)} = \frac{k}{r} \cdot \mathbf{\Omega_r} \left(-Y_k^{(G)}, R_S, Z_k^{(G)}, R_{MO}, k \right). \tag{11}$$

2.2. Magnet Subdomain

Unlike symmetric condition, in the presence of any variation in the geometrical or physical parameter of the magnets, the magnetization vector possesses all integer harmonics k, as depicted by the following expressions:

$$\vec{M}_r(\phi) = \sum_k \left[M_{rc,k} \cos(k\phi) + M_{rs,k} \sin(k\phi) \right] \tag{12}$$

$$\vec{M}_\phi(\phi) = \sum_k \left[M_{\phi c,k} \cos(k\phi) + M_{\phi s,k} \sin(k\phi) \right]. \tag{13}$$

The subscripts (c,k) and (s,k) mean the kth cosine and sine coefficients, respectively. Likewise, the subscripts (a,k) and (b,k) are the kth cosine and sine coefficients of Eqs. (14)–(17)

$$M_{rc,k} = M_{ra,k} \cos(k\phi_r) - M_{rb,k} \sin(k\phi_r) \tag{14}$$

$$M_{rs,k} = M_{ra,k} \sin(k\phi_r) + M_{rb,k} \cos(k\phi_r) \tag{15}$$

$$M_{\phi c,k} = M_{\phi a,k} \cos(k\phi_r) - M_{\phi b,k} \sin(k\phi_r) \tag{16}$$

$$M_{\phi s,k} = M_{\phi a,k} \sin(k\phi_r) + M_{\phi b,k} \cos(k\phi_r). \tag{17}$$

The coefficients for the radial component are shown in Eqs. (18)–(19), while those for the tangential component are Eqs. (20)–(21). The asymmetry is achieved by variations on permanent magnet residual flux $B_{r,j}$ of each magnet j through $M_j = B_{r,j}/\mu_0$, and the tangential offset by δ_j. τ_p is the pole pitch and μ_0 the air magnetic permeability.

$$M_{ra,k} = \sum_{j=0,1,\ldots}^{2p-1} (-1)^j \frac{M_{j+1}}{\pi} \cos\left(kj\tau_p + k\delta_j\right) f_{r,k} \tag{18}$$

$$M_{rb,k} = \sum_{j=0,1,\ldots}^{2p-1} (-1)^j \frac{M_{j+1}}{\pi} \sin\left(kj\tau_p + k\delta_j\right) f_{r,k} \tag{19}$$

$$M_{\phi a,k} = \sum_{j=0,1,\ldots}^{2p-1} (-1)^{j+1} \frac{M_{j+1}}{\pi} \sin\left(kj\tau_p + k\delta_j\right) f_{\phi,k} \tag{20}$$

$$M_{\phi b,k} = \sum_{j=0,1,\ldots}^{2p-1} (-1)^{j+1} \frac{M_{j+1}}{\pi} \cos\left(kj\tau_p + k\delta_j\right) f_{\phi,k}. \tag{21}$$

Functions $f_{r,k}$ and $f_{\phi,k}$ are used to define magnetization patterns according to [10, 12]. The flux

density in the magnet region can be set forth as follows

$$\vec{B}_{r,h}^{(M)} = \sum_k a_{hk}^{(M)} \cos(k\phi) + \sum_k b_{hk}^{(M)} \sin(k\phi) + \sum_k \frac{\mu_0 k}{k^2-1}\Big[(M_{\phi s,hk} + kM_{rc,hk})\cos(k\phi) - (M_{\phi c,hk} - kM_{rs,hk})\sin(k\phi)\Big] \quad (22)$$

$$\vec{B}_{\phi,h}^{(M)} = \sum_k c_{hk}^{(M)} \cos(k\phi) + \sum_k d_{hk}^{(M)} \sin(k\phi) - \sum_k \frac{\mu_0 k}{k^2-1}\Big[(M_{\phi c,hk} - kM_{rs,hk})\cos(k\phi) + (M_{\phi s,hk} + kM_{rc,hk})\sin(k\phi)\Big]. \quad (23)$$

In Eqs. (22)–(23), a_{hk}, b_{hk}, c_{hk} and d_{hk} are functions that enclose the kth Fourier coefficients for each magnet layer h as magnet pole shaping used. In Eqs. (24)–(27), R_M stands for inner and outer radius of magnet layer.

$$a_{hk}^{(M)} = \frac{k}{r} \cdot \mathbf{\Omega_r}\left(Y_{hk}^{(M)}, R_{M,h}, Z_{hk}^{(M)}, R_{M,h-1}, k\right) \quad (24)$$

$$b_{hk}^{(M)} = -\frac{k}{r} \cdot \mathbf{\Omega_r}\left(W_{hk}^{(M)}, R_{M,h}, X_{hk}^{(M)}, R_{M,h-1}, k\right) \quad (25)$$

$$c_{hk}^{(M)} = \frac{k}{r} \cdot \mathbf{\Omega_r}\left(-W_{hk}^{(M)}, R_{M,h}, X_{hk}^{(M)}, R_{M,h-1}, k\right) \quad (26)$$

$$d_{hk}^{(M)} = \frac{k}{r} \cdot \mathbf{\Omega_r}\left(-Y_{hk}^{(M)}, R_{M,h}, Z_{hk}^{(M)}, R_{M,h-1}, k\right) \quad (27)$$

3. STATOR TEETH PAIRING AND NON-UNIFORMLY DISTRIBUTED TEETH

The authors in [6] show that teeth pairing with two different types of tooth width can effectively reduce the cogging torque. In their results, they state that the fundamental or dominant component is completely eliminated although high frequency harmonics are unaffected.

In the same manner, the authors of [8] offer a method that by keeping the center lines of the slots unchanged and shifting only the slot openings, the cogging torque decreases while the three-phase back-EMF is not deteriorated. In the study, the desired shift angle depends upon the number of slots forming the group and the quantity of groups. Also, in accordance with the slot/pole combination, more than one harmonic may be compensated.

On the other hand, a method where one tooth has a different width from the others was proposed in [14]. As a result, the method leads to a geometry where every tooth may be dissimilar to others, since the slot opening of each slot is placed in a different location with respect to the tooth.

In Fig. 1, the major principles of the aforementioned methods are illustrated. A stator with dissimilar teeth is shown in Fig. 1(a), while pairing teeth groups are depicted by Fig. 1(b).

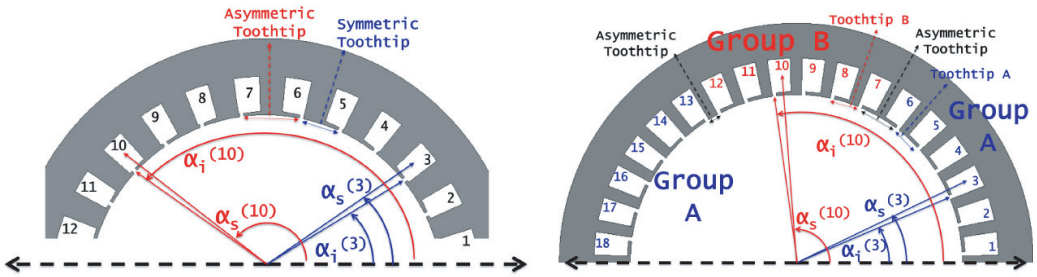

(a) (b)

Figure 1. (a) Non-uniformly distributed stator teeth, (b) stator teeth pairing.

Despite the fact that those techniques exhibit different approaches, they can be indistinctly solved analytically since the subdomain model allows for determining the flux density vector in slot opening whose angle is b_{OA} and slot regions with angle b_{SA}. Therefore, $\alpha_i^{(i)}$ is assumed to be the center of each slot opening for $i = 1, \ldots, N_s$, and the field in the slot opening region remains as

$$\vec{B}_{r,i}^{(SO)} = \sum_m b_{im}^{(SO)} \sin\left(\frac{m\pi}{b_{OA,i}}\left(\phi + \frac{b_{OA,i}}{2} - \alpha_i^{(i)}\right)\right) \tag{28}$$

$$\vec{B}_{\phi,i}^{(SO)} = c_o^{(SO)} + \sum_m c_{im}^{(SO)} \cos\left(\frac{m\pi}{b_{OA,i}}\left(\phi + \frac{b_{OA,i}}{2} - \alpha_i^{(i)}\right)\right), \tag{29}$$

where,

$$c_o^{(SO)} = -\frac{X_i^{(SO)}}{r} \tag{30}$$

$$c_{im}^{(SO)} = -\frac{m}{r}\frac{\pi}{b_{OA,i}} \cdot \mathbf{\Omega_r}\left(Y_{im}^{(SO)}, R_T, -Z_{im}^{(SO)}, R_S, \frac{m}{r}\frac{\pi}{b_{OA,i}}\right). \tag{31}$$

In Eq. (31), R_T is the radius from origin to slot tooth-tip. A new angle $\alpha_s^{(i)}$ is introduced in order to decenter the slot with respect to the slot opening, as follows:

$$\vec{B}_{r,i}^{(S)} = \sum_n b_{in}^{(S)} \sin\left(\frac{n\pi}{b_{SA,i}}\left(\phi + \frac{b_{SA,i}}{2} - \alpha_s^{(i)}\right)\right) \tag{32}$$

$$\vec{B}_{\phi,i}^{(S)} = c_o^{(S)} + \sum_n c_{in}^{(S)} \cos\left(\frac{n\pi}{b_{SA,i}}\left(\phi + \frac{b_{SA,i}}{2} - \alpha_s^{(i)}\right)\right). \tag{33}$$

Expressions (32)–(33) and (34)–(36) are obtained after boundary conditions are applied to ensure tangential continuity of magnetic flux density in the interface slot opening — slot within the range delimited by $\alpha_i^{(i)} - b_{OA,i}/2 \leq \phi \leq \alpha_i^{(i)} + b_{OA,i}/2$. Boundary conditions are applied and serve to calculate the rest of coefficients. R_{SB} is the radius from origin to bottom of the stator slot. J_{i0} and J_{in} are Fourier series coefficients for the current density vector $\vec{J}$ according to [10].

$$b_{in}^{(S)} = -\left[\begin{array}{l} Z_{in}^{(S)}\left(R_{SB}\left(\frac{R_T}{R_{SB}^2}r\right)^{\frac{n\pi}{b_{SA,i}}} + \left(\frac{r}{R_T}\right)^{-\frac{n\pi}{b_{SA,i}}}\right) \\ +\frac{\mu_0 J_{in}}{\left(\frac{n\pi}{b_{SA,i}}\right)^2 - 4}\left(r^2 - \frac{2b_{SA,i}R_{SB}^2}{n\pi}\left(\frac{r}{R_{SB}}\right)^{\frac{n\pi}{b_{SA,i}}}\right) \end{array}\right]\frac{1}{r}\frac{n\pi}{b_{SA,i}} \tag{34}$$

$$c_o^{(S)} = \frac{\mu_0 J_{i0}}{2r}\left(r^2 - R_{SB}^2\right) \tag{35}$$

$$c_{in}^{(S)} = -\left[\begin{array}{l} \frac{2\mu_0 J_{in}}{\left(\frac{n\pi}{b_{SA,i}}\right)^2 - 4}\left(r - \frac{R_{SB}^2}{r}\left(\frac{r}{R_{SB}}\right)^{\frac{n\pi}{b_{SA,i}}}\right) \\ +\frac{n}{r}\frac{Z_{in}^{(S)}\pi}{b_{SA,i}}\left(R_{SB}\left(\frac{R_T}{R_{SB}^2}r\right)^{\frac{n\pi}{b_{SA,i}}} - \left(\frac{r}{R_T}\right)^{-\frac{n\pi}{b_{SA,i}}}\right) \end{array}\right] \tag{36}$$

4. TANGENTIAL SHIFT OF MAGNETS AND NON-UNIFORM MAGNET WIDTH

By independently manipulating the geometry and placement of magnets in PMSMs, performance improvements can also be fulfilled. Bianchi and Bolognani discuss several techniques for reducing

cogging torque in [1], and some of these methods include PM arc with different widths and tangential shifting of magnets in Figs. 2(b) and 2(a), respectively.

Posteriorly, further studies in the search for the optimum PM arc and shifting angle have been carried out by [4, 15, 16]. All of them are conducted with different geometries and slot/pole combinations; however, all of them agree that, by asymmetrical placement of magnet, harmonics with the same order can be arranged such that the magnitude is compensated by means of opposing its phases.

Likewise, the authors in [13] state that even suppressing the cogging torque, the torque ripple at rated operation condition may be still large and unacceptable because minimizing cogging torque cannot certainly reduce torque ripple. Therefore, they introduce a method where the width of only one magnet is different from the others. Among the findings, there is an important drawback that the UMP is greatly increased by this technique.

In Fig. 2(a), groups of magnets can be arranged according to the slot/pole combination and optimum shifting angle. Similarly, Fig. 2(b) shows an arrangement of magnets where one of them has a dissimilar arc length, that is to say, $\beta_3 = \beta_2 \neq \beta_1$.

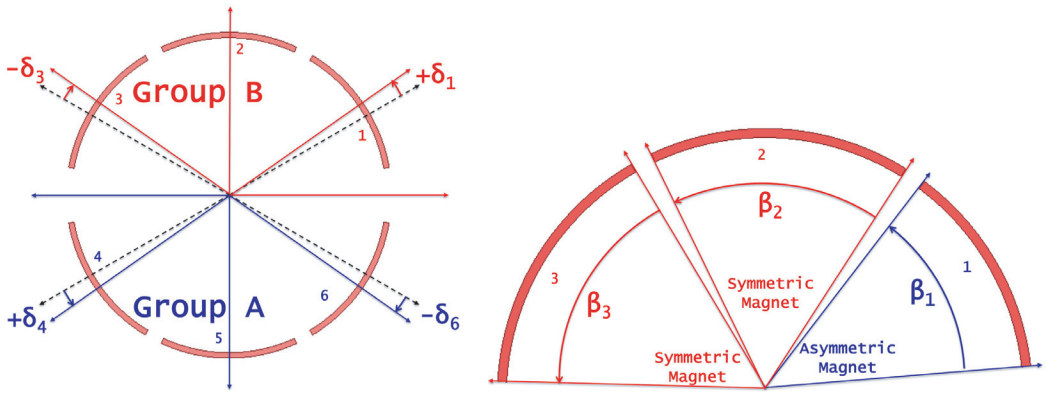

(a) (b)

Figure 2. (a) Tangential shifting of magnets, (b) dissimilar magnet arc.

The asymmetry in magnets is achieved analytically through the radial and tangential components of magnetization vector $(\vec{M}_r, \vec{M}_\phi)$ as aforementioned.

Hence, functions $f_{r,k}$ and $f_{\phi,k}$ describe the radial in Eq. (39) and parallel magnetization in Eqs. (37)–(38), where independent arc lengths $\beta_m^{(j)}$ are introduced to account for magnets with nonuniform width (arc length).

$$f_{r,k} = \begin{cases} \dfrac{\sin\left((k-1)\,\beta_m^{(j)}\right)}{2(k-1)} + \dfrac{\sin\left((k+1)\,\beta_m^{(j)}\right)}{2(k+1)}, & k \neq 1 \\ \dfrac{1}{2}\sin\left(\beta_m^{(j)}\right) - \beta_m^{(j)} \quad , & k = 1 \end{cases} \tag{37}$$

$$f_{\phi,k} = \begin{cases} \dfrac{\sin\left((k+1)\,\beta_m^{(j)}\right)}{2(k+1)} - \dfrac{\sin\left((k-1)\,\beta_m^{(j)}\right)}{2(k-1)}, & k \neq 1 \\ \dfrac{1}{2}\sin\left(\beta_m^{(j)}\right) - \beta_m^{(j)} \quad , & k = 1 \end{cases} \tag{38}$$

$$f_{r,k} = f_{\phi,k} = 2\frac{\sin\left(0.5k\beta_m^{(j)}\right)}{k}. \tag{39}$$

5. SIMULATION RESULTS

Two geometries, as shown in Fig. 3, have been selected to show the validity of the proposed model on predicting the effect of geometrical asymmetries in the spatial harmonics of the flux density. A complete list of motor parameters is given in Table A1. Consequently, the machine performance is further enhanced, and particularly, cogging torque and back-EMF results are studied in this work. Flux density in the air gap is attained from proposed model, and then torque is calculated according to Maxwell stress theory in Eq. (40), where L_{stk} is the motor stack length, r_g the radius at the middle of air gap, and ϕ_r the rotor position.

$$T = \frac{L_{stk} r_g^2}{\mu_0} \int_0^{2\pi} \vec{B}_r^{(G)} \vec{B}_\phi^{(G)} d\phi_r \tag{40}$$

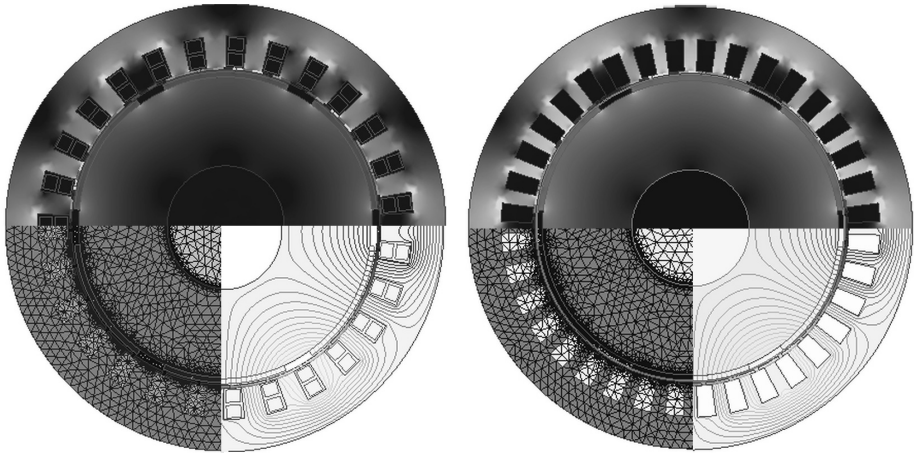

(a) (b)

Figure 3. PMSMs with 6 magnet poles, (a) 27 slots, and (b) 36 slots for validation.

5.1. Stator Asymmetry

The stator of the machine with 27 slots is modified according to the method of nonuniformly distributed teeth. Hence, the new stator has one toothtip with arc length different from the other 26 teeth, as illustrated by Fig. 1(a). The arc length in degrees for the asymmetric toothtip is 17.9°, while the other 26 teeth have an arc length of 11.7°.

The model solves such geometry by defining the center position of each slot opening and the center of stator slots independently, as can be seen in Table 1. The table shows that 26 out of 27 slot openings are equally separated at about 13.1°, and one toothtip is asymmetric, that of placed between slot openings 17 and 18, which are spaced at about 19.36°. Contrastingly, all the stator slots keep equidistant by $360/N_s$ degrees.

Table 1. Stator with non-uniformly distributed teeth, slot openings and slot positions.

Slot	**Angle between Slot openings** (°)	**Angle between Slots** (°)
1–17	13.1	13.33
17–18	19.36	13.33
18–27	13.1	13.33

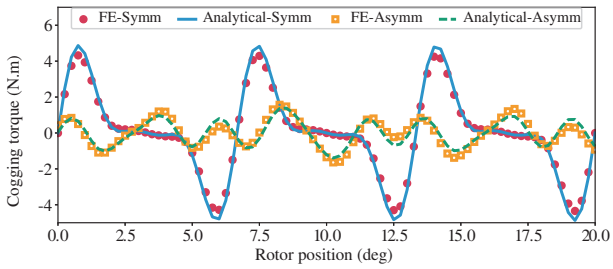

Figure 4. Compensation in 27-slots/6-poles by non-uniformly distributed stator teeth.

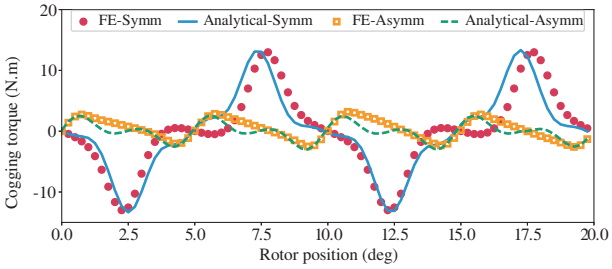

Figure 5. Compensation in 36-slots/6-poles by stator teeth pairing.

As a result, the cogging torque is calculated and compared against FE-based models, and the results are reported in Fig. 4, where the effective diminution of cogging torque compared to a symmetric model can be firstly observed, in which slots and slots opening are equidistant by 13.33°, and the reduction is about 65%. Secondly, agreement between results from analytical and numerical methods is observed.

Table 2. Stator with teeth pairing, slot openings and slot positions.

Slot	Angle between Slot openings (°)	Angle between Slots (°)
1–6	10.0	10.0
6–7	15.0	10.0
7–12	10.0	10.0
12–13	5.0	10.0
13–18	10.0	10.0
18–19	15.0	10.0
19–24	10.0	10.0
24–25	5.0	10.0
25–30	10.0	10.0
30–31	15.0	10.0
31–36	10.0	10.0

For the second verification in terms of asymmetric stators, the teeth pairing method is applied to a machine with 36-slots/6-poles, as illustrated by Fig. 3(b). In this machine, six groups of stator teeth are identified where three belong to group A and the other three to group B, as observed in Fig. 1(b). Slot openings of group A are shifted clockwise while those of group B are rotated counterclockwise, and both groups are shifted 2.5°, respectively. As a result, six groups with six teeth each are arranged such that the slot openings are centered according to Table 2. It can also be observed that stator slots are equally spaced by $360/N_s$ degrees.

The results in Fig. 5 show agreement between FE and analytic model; furthermore, the suppression in cogging torque by this method is 75%.

5.2. Rotor Asymmetry

Similarly, rotor asymmetry by tangential shifting of permanent magnets is verified. This method is applied to the 27-slots/6-poles machine in which the stator is kept unchanged (symmetric) while PMs are rotated by angle δ_j, as illustrated by Fig. 2(a). The exact location of each magnet is reported in Table 3, and magnet arc length is the same for all.

Table 3. Tangential displacement of magnets in machine with 27-sots/6-poles.

	Permanent Magnets					
Angle	**1**	**2**	**3**	**4**	**5**	**6**
δ_j (°)	+4.44	0.00	−4.44	+4.44	0.00	−4.44

Table 4. Arc length of magnets with non-uniform width of machine with 36-sots/6-poles.

	Permanent Magnets					
Angle	**1**	**2**	**3**	**4**	**5**	**6**
$\beta_m^{(j)}$ (°)	46.87	56.87	56.87	56.87	56.87	56.87

After modeling the machine with both methods, cogging torques are computed and compared in Fig. 6. By tangential shifting of magnets, the reduction in cogging torque achieved with respect to the initial design (symmetric) is 84%. Fair agreement between the solutions is observed as well.

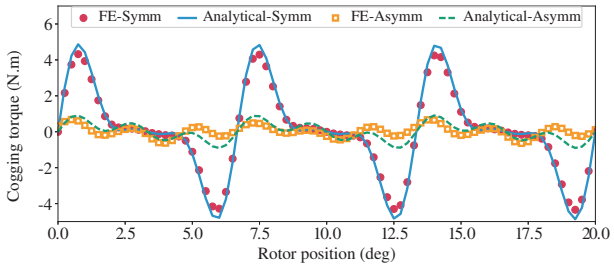

Figure 6. Compensation in 27-slots/6-poles by non-uniformly distributed magnets.

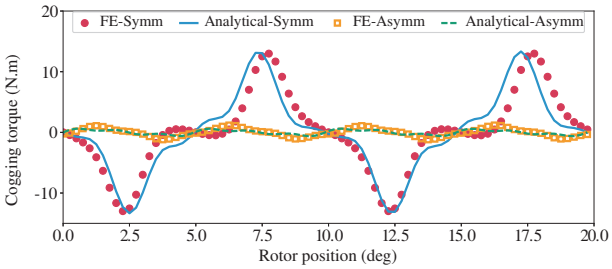

Figure 7. Compensation in 36-slots/6-poles by using permanent magnets with non-uniform width.

The next technique utilized to verify the validity of the model is that proposed by [13], where only one magnet width may be narrower or wider while the others have constant arc β_m. For such a purpose, the machine with 36 symmetric slots is selected as PMs are arranged according to Fig. 2(b). More details with respect to the dissimilar magnet widths are depicted in Table 4.

Both examples of rotor asymmetry are simulated with radial magnetization; nonetheless, the results can be applied and extended to more magnetization patters by redefining the functions of magnetization in Eqs. (37)–(39).

When the latter method is employed, the cogging torque decreases in 90% of the symmetrical machine, as shown in Fig. 7, and the proposed method also follows the trend with the added benefits of quickness in the solution and free of meshing errors.

5.3. Effects on Back-EMF

Parasitic torque in Surface Permanent Magnet motors (SPM) is mostly influenced by cogging torque and back-EMF harmonics. If saturation is neglected, and the magnetic materials of the machine operate mainly in the linear region of the induction curve, torque ripple can be predicted by summation of cogging torque and interaction of back-EMF harmonics with fundamental component of stator current.

Therefore, a common practice in the industry is to measure and ensure that back-EMF harmonics are below certain threshold in order to meet application requirements, specially applications for which smooth torque is mandatory, such as servo-motors, robotics, electric power steering, and traction motors

in electric vehicles.

Back-EMF waveforms are also calculated with the proposed model according to Eq. (41), where ω_r is the mechanical speed, N the number of turns per coil, and r_s the integration radius near inner stator.

$$E = -\omega_r N \frac{\partial}{\partial \phi_r} \left[L_{stk} r_s \int_0^{2\pi} \vec{B}_r^{(G)} w_{abc} d\phi \right] \tag{41}$$

Likewise, winding function w_{abc} sets forth the conductor density placed in stator slots [7]. Fourier series can be used to define winding functions for machines with either concentrated or distributed stator wound.

The good agreement between calculated back-EMF at 1000 rpm and that simulated with FE method is worth noting, as shown in the results. Fig. 8 depicts the back-EMF obtained from the conventional motor with 27-slots/6-poles as no asymmetry is introduced. For instance, slots and slot openings are equidistant at 13.33° from one another. Furthermore, all magnets have the same size and are 60° apart.

The winding for all the variants of 27-slots/6-poles motors consists of nine coils in series per phase. Each coil has seven turns, and their pitch is five slots. In Fig. 9, the results are shown for the geometry with rotor asymmetry where magnet placement is according to Table 3. On the other hand, as stator with nonuniformly distributed teeth is used, the resultant back-EMF has higher harmonic content than that of rotor asymmetry, as can be seen in Fig. 10, which agrees with the results observed in cogging torque.

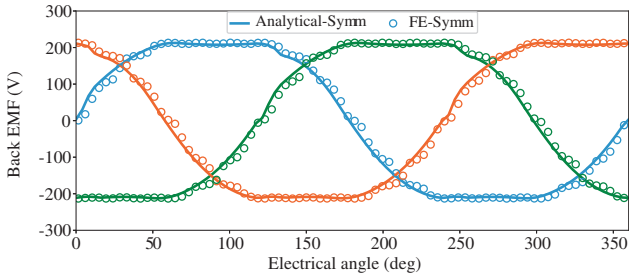

Figure 8. Back-EMF in 27-slots/6-poles with symmetry in both stator and rotor.

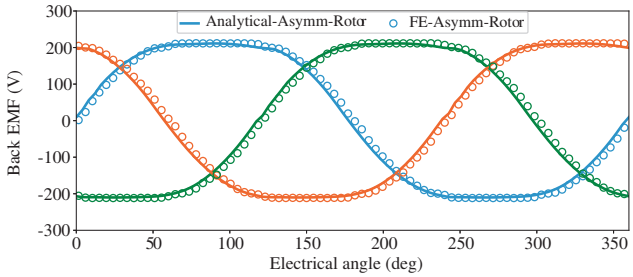

Figure 9. Back-EMF in 27-slots/6-poles with asymmetry in rotor by non-uniformly distributed magnets.

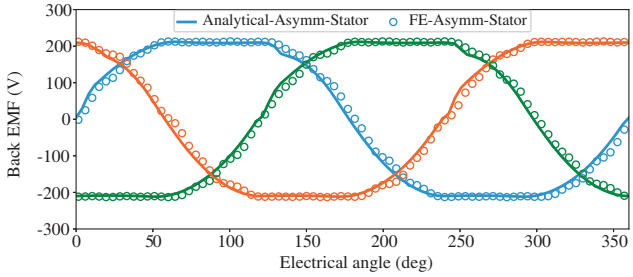

Figure 10. Back-EMF in 27-slots/6-poles with asymmetry in stator by non-uniformly distributed teeth.

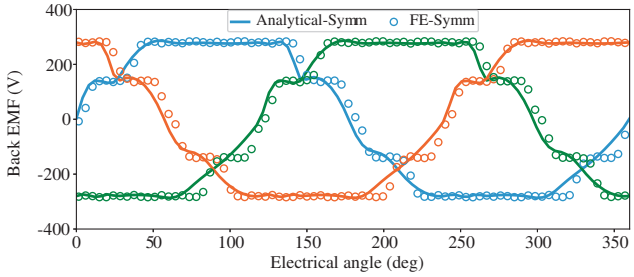

Figure 11. Back-EMF in 36-slots/6-poles with symmetry in both stator and rotor.

As for the 36-slots/6-poles, Fig. 11 shows results for the symmetrical machine. The winding consists of twelve coils in series per phase. Each coil has seven turns, and coil pitch is equal to six. The rotor asymmetry is introduced by means of magnets with different widths. Particularly, magnet one has arc angle of 46.87° while others have 56.87°, and back-EMF waveforms are reported on Fig. 12. Finally, teeth pairing technique is also calculated with the proposed model and simulated numerically, and the agreement is depicted in Fig. 13 according to stator teeth grouped as stated in Table 2.

Comparing the techniques, it can be withdrawn that the lowest back-EMF deterioration is obtained with tangential shift of magnets and stator teeth pairing. Nevertheless, magnet shift further punishes the fundamental component of back-EMF which implies significant reduction of average torque.

Geometry with dissimilar tooth-tips does not considerably affect back-EMF as observed in Table 5. On the other hand, uneven magnet width strategy shows the largest back-EMF distortion although it is noteworthy that the major contributor is the 3rd order harmonic and can be reduced through wye connections, as can be observed on harmonic spectra in Fig. 14 and Fig. 15. The increase of 6% in the fundamental back-EMF observed in the 36-slots/6-poles with rotor asymmetry is due to 19% more permanent magnet material.

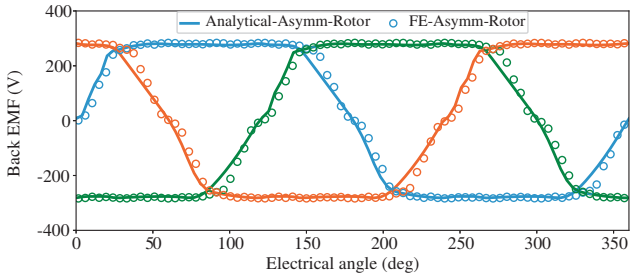

Figure 12. Back-EMF in 36-slots/6-poles with asymmetry in rotor through magnets with non-uniform width.

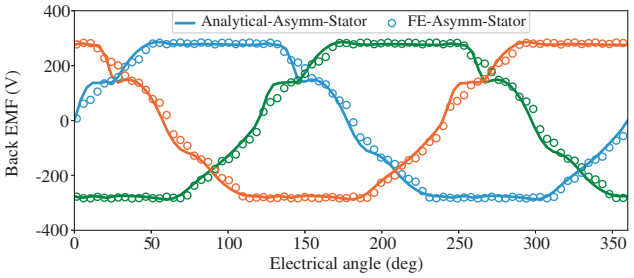

Figure 13. Back-EMF in 36-slots/6-poles with asymmetry in stator through teeth pairing.

Table 5. Fundamental and THD in back EMF.

Description	27-slots/6-poles		36-slots/6-poles	
	Fundamental (V)	THD (%)	Fundamental (V)	THD (%)
Symmetrical	243.32	13.87	322.97	16.43
Rotor asymmetry	238.99	11.70	340.84	23.15
Stator asymmetry	243.34	13.75	319.14	11.73

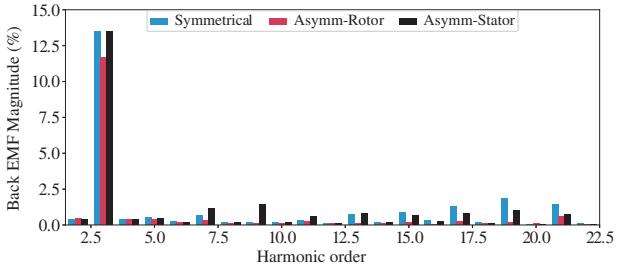

Figure 14. Comparison of Back-EMF harmonics in 27-slots/6-poles, as percentage of fundamental. Geometry with symmetry against that of rotor with shifted magnets and asymmetrical stator tooth-tip.

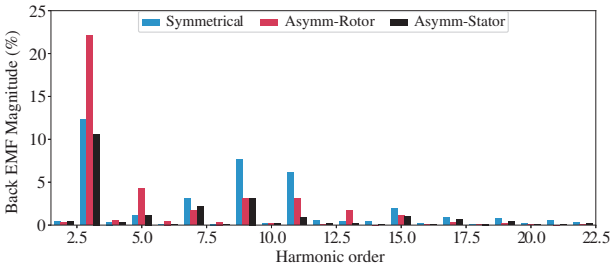

Figure 15. Comparison of Back-EMF harmonics in 36-slots/6-poles, as percentage of fundamental. Geometry with symmetry against that of rotor with uneven magnet widths and stator teeth pairing.

6. CONCLUSIONS

This work proves that the effective usage of asymmetries in either stator or rotor leads to reduced pulsating of PMSMs.

Because asymmetric geometries exhibit more parameters to be searched for and optimized, the design process is expected to be longer than a conventional model. For that reason, a worthy analytic tool is presented and validated in this paper to speed up the analysis of such problems. The analytical results reported in this work are obtained in an average of 2 seconds when using 100 harmonics in the air gap, while numerical simulations last for several minutes depending on mesh resolution, and unfortunately, periodicity cannot be used to reduce the FE model.

With the aid of examples provided in this paper, it has been corroborated that reduction in cogging torque of 65%–75% can be fulfilled by appropriately introducing asymmetries in the stator, particularly, at slot opening position. Similarly, the cogging torque as employing rotor asymmetry shows between 84%–90% lower amplitude than that of the symmetrical case. With regards to THD of back-EMF, tangential magnet shift reduces harmonic content in 2.17% while stator teeth pairing enhances it in 4.7%.

It is noteworthy that tremendous improvements are observed; however, the compensation of spatial harmonics occurs in the resultant tangential forces. Having said that, the study of radial forces and their consequences in the UMP in utilizing any of these techniques are important. Additionally, rotor asymmetry may offset the rotor center of mass, if care is not taken.

APPENDIX A. VALIDATION MOTORS

Table A1. Main parameters of validation SPM motors.

Parameter	Fig. 3(a) 27-slots/6-poles	Fig. 3(b) 36-slots/6-poles
Slots	27	36
Poles	6	6
Stator outer radius	170.00 mm	170.00 mm
Stator inner radius	119.00 mm	119.00 mm
Stack Length	160.00 mm	160.00 mm
Tooth width	13.90 mm	10.00 mm
Slot opening width	3.00 mm	3.00 mm
Magnet length	4.00 mm	4.00 mm
Rotor outer radius	113.50 mm	113.50 mm
Tooth tip height	2.00 mm	2.00 mm
Magnet arc length	145.8°	136.8°
Residual flux	1.23 T	1.23 T
Magnet permeability	1.10	1.10
Magnetization	Radial	Radial

REFERENCES

1. Bianchi, N. and S. Bolognani, "Design techniques for reducing the cogging torque in surface-mounted," *IEEE Trans. Ind. Appl.*, Vol. 38, No. 5, 1259–1265, Sep. 2002.
2. Bianchi, N. and S. Bolognani, "Reduction of cogging force in PM linear motors by pole-shifting," *IEE Proceedings — Electric Power Applications*, 703–709, 2005.

3. Bianchi, N., S. Bolognani, D. Bon, and M. D. Pr, "Torque harmonic compensation in a synchronous reluctance motor," *IEEE Trans. Energy Convers.*, Vol. 23, No. 2, 466–473, 2008.
4. Dosiek, L. and P. Pillay, "Cogging torque reduction in permanent magnet machines," *IEEE Trans. Ind. Appl.*, Vol. 43, No. 6, 1565–1571, 2007.
5. Gysen, B. L. J., K. J. Meessen, J. J. H. Paulides, and E. A. Lomonova, "General formulation of the electromagnetic field distribution in machines and devices using fourier analysis," *IEEE Trans. Magn.*, Vol. 46, No. 1, 39–52, 2010.
6. Hwang, S.-M., J.-B. Eom, G.-B. Hwang, W.-B. Jeong, and Y.-H. Jung, "Cogging torque and acoustic noise reduction in permanent magnet motors by teeth pairing," *IEEE Trans. Magn.*, Vol. 36, No. 5, 3144–3146, 2000.
7. Krause, P., O. Wasynczuk, S. D. Sudhoff, and S. Pekarek, *Analysis of Electric Machinery and Drive Systems*, IEEE Press Series on Power Engineering, Wiley, 2013.
8. Liu, T., S. Huang, J. Gao, and K. Lu, "Cogging torque reduction by slot-opening shift for permanent magnet machines," *IEEE Trans. Magn.*, Vol. 49, No. 7, 4028–4031, 2013.
9. Pfister, P.-D. and Y. Perriard, "Slotless permanent-magnet machines: General analytical magnetic field calculation," *IEEE Trans. Magn.*, Vol. 47, No. 6, 1739–1752, Jun. 2011.
10. Piña, A. and L. Xu, "Analytical prediction of torque ripple in surface-mounted permanent magnet motors due to manufacturing variations," *IEEE Trans. Energy Convers.*, Vol. 31, No. 4, 1634–1644, 2016.
11. Piña, A. and L. Xu, "Investigation of effects of asymmetries on the performance of permanent magnet synchronous machines," *IEEE Trans. Energy Convers.*, Vol. PP, No. 99, 1–1, 2017.
12. Piña, A., S. Paul, R. Islam, and L. Xu, "Analytical model for predicting effects of manufacturing variations on cogging torque in surface-mounted permanent magnet motors," *IEEE Trans. Ind. Appl.*, Vol. 52, No. 4, 3050–3061, 2016.
13. Wang, D., X. Wang, and S. Y. Jung, "Cogging torque minimization and torque ripple suppression in surface-mounted permanent magnet synchronous machines using different magnet widths," *IEEE Trans. Magn.*, Vol. 49, No. 5, 2295–2298, 2013.
14. Wang, D., X. Wang, D. Qiao, Y. Pei, and S. Y. Jung, "Reducing cogging torque in surface-mounted permanent-magnet motors by nonuniformly distributed teeth method," *IEEE Trans. Magn.*, Vol. 47, No. 9, 2231–2239, 2011.
15. Wang, D., X. Wang, Y. Yang, and R. Zhang, "Optimization of magnetic pole shifting to reduce cogging torque in solid-rotor permanent-magnet synchronous motors," *IEEE Trans. Magn.*, Vol. 46, No. 5, 1228–1234, May 2010.
16. Yang, Y., X. Wang, C. Zhu, and C. Huang, "Study of magnet asymmetry for reduction of cogging torque in permanent magnet motors," *IEEE Conference on Industrial Electronics and Applications*, Vol. 2, 2325–2328, 2009.